

Geophysical Research Letters

RESEARCH LETTER

10.1029/2025GL116020

Key Points:

- · Upwind of postfrontal clouds we identify a daytime increase in nucleation mode aerosol diameter and accumulation mode number concentration
- Observational constraints based on ACTIVATE aircraft data and satellite retrievals indicate a moderate aerosol hygroscopicity ($\kappa = 0.3$)
- Increased afternoon accumulation mode concentrations facilitate an updraft-limited regime that curbs activation of Aitken mode aerosol

Supporting Information:

Supporting Information may be found in the online version of this article.

Correspondence to:

F. Tornow. ft2544@columbia.edu

Citation:

Tornow, F., Crosbie, E. C., Fridlind, A. M., Ackerman, A. S., Ziemba, L. D., Elsaesser, G., et al. (2025). High accumulation mode aerosol concentration and moderate aerosol hygroscopicity limit impacts of recent particle formation on Northwest Atlantic post-frontal clouds. Geophysical Research Letters 52 e2025GL116020 https://doi.org/10.1029/2025GL116020

Received 17 MAR 2025 Accepted 24 JUL 2025

Author Contributions:

Conceptualization: F. Tornow Data curation: F. Tornow Formal analysis: F. Tornow, E. C. Crosbie, A. M. Fridlind, A. S. Ackerman, L. D. Ziemba, S. Chellappan, P. Zuidema Funding acquisition: A. Sorooshian Investigation: F. Tornow

Methodology: F. Tornow, E. C. Crosbie, A. M. Fridlind

Project administration: A. Sorooshian Resources: F. Tornow Software: F. Tornow

© 2025. The Author(s). This is an open access article under the terms of the Creative Commons Attribution License, which permits use, distribution and reproduction in any medium, provided the original work is properly cited.

High Accumulation Mode Aerosol Concentration and Moderate Aerosol Hygroscopicity Limit Impacts of Recent Particle Formation on Northwest Atlantic Post-Frontal **Clouds**

F. Tornow^{1,2} , E. C. Crosbie^{3,4} , A. M. Fridlind² , A. S. Ackerman² , L. D. Ziemba³ , G. Elsaesser^{2,5} , B. Cairns², D. Painemal^{3,4}, S. Chellappan^{3,4} , P. Zuidema⁶ , C. Voigt^{7,8} , S. Kirschler^{7,8} , and A. Sorooshian⁹

¹Earth Institute, Columbia University, New York, NY, USA, ²NASA Goddard Institute for Space Studies, New York, NY, USA, ³NASA Langley Research Center, Hampton, VA, USA, ⁴Analytical Mechanics Associates, Hampton, VA, USA, ⁵The Department of Applied Physics and Applied Mathematics, Columbia University, New York, NY, USA, ⁶Rosenstiel School of Marine, Atmospheric and Earth Science, University of Miami, Miami, FL, USA, ⁷Deutsches Zentrum für Luftund Raumfahrt (DLR), Oberpfaffenhofen, Germany, ⁸Johannes Gutenberg-Universität, Mainz, Germany, ⁹Department of Chemical and Environmental Engineering, University of Arizona, Tucson, AZ, USA

Abstract Postfrontal cloud regime transitions often result from strong aerosol-cloud-precipitation interaction. Using ACTIVATE measurements from 40 flights, we show a diurnal pattern of evolving aerosol particle size distributions (PSD) in the marine boundary layer upwind of clouds. A nucleation mode grows in size between 12 and 17 LT, likely from new particle formation (NPF), and an accumulation mode increases in concentration during daytime. Selecting the day of strongest size growth, we use quasi-Lagrangian large-eddy simulations to examine cloud impacts. With a morning PSD, moderate aerosol hygroscopicity aligns best with satellite and field campaign observational targets. Using a PSD near 17 LT, greater cloud droplet number concentrations delay the precipitation onset and keep albedo elevated for longer, primarily driven by increased accumulation mode concentrations, which facilitate an updraft-limited regime and inhibit activation of smaller modes despite their growth after NPF. These results constitute a caveat for NPF-related activation under polluted conditions.

Plain Language Summary Cloud breakup in the postfrontal sector of extratropical cyclones is often the result of precipitation. Once precipitating, the marine boundary layer (MBL) stabilizes as partial evaporation of precipitation cools and moistens the sub-cloud layer. In addition, aerosol available as cloud condensation nuclei decreases in number during precipitation-forming collisional events. Here we use multiple years of flight measurements collected over the Northwest Atlantic. Inside the MBL we reveal a diurnal pattern of evolving aerosol properties before clouds are forming: very small particles (diameters smaller 10 nm), so called nucleation mode aerosol, grow in diameter over the course of each day while medium-sized particles (diameters greater 80 nm), so called accumulation mode aerosol, increase in number. In order to understand if grown nucleation mode particles may impact clouds, we perform large-eddy simulations that follow an MBL air mass. Using aerosol prior to growth, we find that their ability to attach condensate is generally moderate, evidenced by a better agreement to field and satellite data. When switching to the time period after aerosol growth, simulations show brighter clouds that begin precipitating later, which we attribute to increased accumulation mode concentrations that are numerous enough to inhibit activation of grown nucleation mode aerosol.

1. Introduction

The interaction of aerosol, clouds, and precipitation commonly plays a leading role in regime transitions in marine low-level clouds (e.g., Eastman et al., 2022), which substantially lower regional albedo through a decrease in cloud fraction and cloud optical depth (COD) and a change in cloud morphology from an overcast towards a typically open-cellular state (D. T. McCoy et al., 2023). These transitions result from a progressive stabilization of the marine boundary layer (MBL) under the cooling and moistening from evaporating precipitation, thereby bottling up warm and moist air in the lower MBL where surface fluxes are great (Grossman & Betts, 1990) and causing dynamics of an increasingly convective nature. An intrinsic part of precipitation-induced cloud regime

TORNOW ET AL. 1 of 12 Supervision: E. C. Crosbie,
A. M. Fridlind, A. S. Ackerman
Validation: F. Tornow, G. Elsaesser,
D. Painemal, C. Voigt, S. Kirschler
Visualization: F. Tornow
Writing – original draft: F. Tornow,
E. C. Crosbie, A. M. Fridlind
Writing – review & editing: F. Tornow,
E. C. Crosbie, A. M. Fridlind,
L. D. Ziemba, G. Elsaesser, B. Cairns,
D. Painemal, S. Chellappan, P. Zuidema,
C. Voigt, S. Kirschler, A. Sorooshian

transitions is the efficient removal of aerosol (Wood et al., 2017) serving as cloud condensation nuclei (CCN) via precipitation formation (e.g., Yamaguchi et al., 2017). Fewer CCN result in lower cloud droplet number concentrations and maintain or even amplify precipitation for any given amount of cloud condensate (e.g., Comstock et al., 2004; Wood, 2005). Given the involvement of many microphysical processes necessary to plausibly capture these regime transitions, it is unsurprising that models exhibit radiative biases when compared against observational benchmarks (Tselioudis et al., 2021). Postfrontal clouds including mid-latitude marine cold-air outbreaks (MCAOs) are particularly vital to better understand as their undetermined cloud feedback dominates the uncertainty in projected global mean temperature (Zelinka et al., 2020).

The recent NASA Aerosol Cloud meTeorology Interactions oVer the western ATlantic Experiment (ACTIVATE, Sorooshian et al., 2019; Sorooshian et al., 2025) campaign over the Northwest Atlantic probed many MCAOs and enables a better understanding of the evolution of microphysical properties with fetch. For example, recent work revealed the omnipresence of mixed-phase condensate (Seethala et al., 2024) that is expected to accelerate cloud regime transitions via riming (Tornow et al., 2021). Because of ACTIVATE's proximity to upwind natural and anthropogenic emission (e.g., Liu et al., 2024), MBL aerosol concentrations are comparatively large (e.g., Sanchez et al., 2023) and strong entrainment of relatively clean free tropospheric (FT) air has been shown to dominate the reduction in MBL CCN concentrations upwind of substantial rain onset and associated cloud regime transitions (Tornow et al., 2022). Regional aerosol hygroscopicity, as quantified via the κ parameter, has been reported to range anywhere between 0.05 and 0.70 (e.g., Phillips et al., 2018), with continental air typically being less hygroscopic than marine ones (e.g., Kuang et al., 2020). The interface of MBL and FT also exhibits favorable conditions for new particle formation (NPF, Corral et al., 2022; Namdari et al., 2024). Nucleation mode aerosol (here defined as particle diameters $D_p < 10$ nm) that typically grow in size to become Aitken mode particles (here defined as $D_p \in 10$ –80 nm) may serve as CCN (e.g., Gordon et al., 2017) and are hypothesized to buffer cloud droplet number concentrations (I. L. McCoy et al., 2024) much farther downwind, where postfrontal air typically arrives cleansed (e.g., Wood et al., 2017). NPF is expected to constitute a sizable portion of CCN (Zhao et al., 2024). Given the overall decrease in AOD over the ACTIVATE domain in the past two decades (e.g., Park et al., 2024), the role of smaller particles to potentially serve as CCN should increase even in relatively polluted

This paper compiles in situ observations throughout the ACTIVATE deployment to reveal a persistent diurnal pattern (here defined as the difference between morning and afternoon conditions) of particle size growth in the clear MBL upwind of postfrontal cloud formation. We then use an exemplary case of strong size growth as input to large eddy simulations (LES) in order to understand the potential role of size-grown and newly formed particles to supplement CCN. Our main goal is to understand the impact of evolving upwind aerosol on the downwind cloud deck. The paper is organized as follows: Section 2 explains field as well as satellite data and quasi-Lagrangian LES, Section 3 compares simulations that were initialized using a range of observed aerosol properties, Section 4 discusses the findings, and Section 5 provides conclusions.

2. Data and Methodology

2.1. ACTIVATE Flight Measurements

ACTIVATE sampled aerosol, clouds, and dynamic and thermodynamic properties during several deployments between 2020 and 2022. Extensive details about the ACTIVATE flight and instrument details are provided elsewhere (Sorooshian et al., 2023). Winter deployments mainly targeted postfrontal areas of extratropical cyclones, resulting in 72 flights over the course of 47 days across the entire period (Tornow, Fridlind, et al., 2025), as listed in Table S1 in Supporting Information S1. Most flights were performed in tandem, with a low-flying aircraft that probed clouds and aerosol in situ and a high-flying aircraft carrying remote sensing instruments and launching dropsondes. Text S1c in Supporting Information S1 provides a detailed overview of key instruments utilized in this paper.

To classify in situ flight legs, we mainly follow the approach from Tornow et al. (2022), except we here use longer horizontal legs that typically span \sim 3–6 min or about \sim 20–40 km. As explained in more detail in Text S1a in Supporting Information S1, we use liquid water content to filter for legs free of cloud condensate. To decide whether a clear leg belongs to MBL or FT, we utilize the altitude of nearby cloudy legs (assuming that there are no

TORNOW ET AL. 2 of 12

clouds in the FT), informed by in situ probes as well as cloud-top height, measured by High Spectral Resolution Lidar 2 (HSRL-2, Burton et al., 2018).

To compute each leg's fetch, which is here defined as the downwind distance from the apparent location of cloud formation, we again follow the approach from Tornow et al. (2022) that is explained in greater detail in Text S1b in Supporting Information S1: geostationary satellite imagery from the 16th Geostationary Operational Environmental Satellites East (GOES-16) taken at about median flight time allows for drawing a great circle line along locations where clouds first appear, providing plausible geo coordinates beyond the domain of interest; together with a wind vector extracted from ERA5 reanalysis (Hersbach et al., 2020), we compute the projected distance upor downwind from the great circle.

Central aspects rely on in situ probed aerosol measurements. As explained in greater detail in Text S1c in Supporting Information S1, we merge aerosol particle size distribution measured from a laser aerosol spectrometer (LAS) and a scanning mobility particle sizer (SMPS). In addition, we utilize measurements of total and non-volatile particle number concentrations, to isolate aerosol size distributions with low non-volatile fractions and to minimize contributions from primary combustion sources. We also compute theoretical activation for a given supersaturation via simplified Koehler theory, by first fitting log-normal modes to PSDs and then assuming mode-specific hygroscopicity, κ .

Lastly, we compile observational constraints from ACTIVATE measurements. We use a Lagrangian trajectory extracted from ERA5 (Text S1e in Supporting Information S1) and collect all in situ and remote sensing measurements collected within 60 min and 100 km of the trajectory. To compile statistics equivalent to LES domain statistics, we average remote sensing data from the upper aircraft over 5 min periods (roughly translating into 30 km intervals). Collocated ACTIVATE measurements are shown in Figure S4 in Supporting Information S1.

2.2. Observational Constraints From Satellite Retrievals

To evaluate simulated cloud fields, we collect retrievals from low-earth-orbiting satellites, following Tornow et al. (2023), which include instantaneous MAC-LWP (Multi-Sensor Advanced Climatology of Liquid Water Path, Elsaesser et al., 2017) total liquid water paths, and MODIS (Moderate Resolution Imaging Spectroradiometer) and VIIRS (Visible Infrared Imaging Radiometer Suite) COD and cloud-top effective radius to compute cloud droplet number concentration (Painemal & Zuidema, 2011). In addition, we use COD from GOES-16 at day and night to produce cloud cover every 20 min, measured as the portion of pixels with COD > 2.5 (Wyant et al., 1997) to be consistent with LES. Nighttime COD retrievals rely on three thermal channels (Minnis & Heck, 2012). To account for heterogeneous cloud fields, we compute cloud cover as the fraction of pixels with COD greater 2.5 over a (25 km)² sliding window. All other quantities are computed as simple arithmetic means. All satellite products are collected within 50 km of the trajectory location at the time of acquisition, forming a domain of (100 km)².

2.3. DHARMA Large-Eddy Simulations

Quasi-Lagrangian large-eddy simulations (LES) translate with the boundary layer air mass away from the eastern seaboard, thereby following the general setup of Tornow et al. (2021, 2023). Like before, we use a domain size of $(21 \text{ km})^2$ resolved at 150 m and 5 km depth resolved through 200 layers. An exception to previous quasi-Lagrangian LES is the use of multiple lognormal aerosol modes instead of one. These modes are fitted from ACTIVATE-measured PSDs (see Section 2.1 and Text S1c in Supporting Information S1) and span the geometric diameters between 16 and 210 nm (see Table S2 in Supporting Information S1). Another exception to previous simulations is the use of the Hallet-Mossop secondary ice production mechanism, active when substantial rain (RWP > 25 g m⁻²) is forming. We note that rime-splintering remains an uncertain process (Seidel et al., 2024), whereas other potentially strong secondary ice production mechanisms also remain poorly established (e.g., Korolev et al., 2024).

3. Results

3.1. Growth of Newly Formed Particles Upwind of Clouds

From ACTIVATE's multi-year deployment, we select 72 flights during postfrontal conditions (Tables S1 and S2 in Supporting Information S1). Most flights show southeastward flow at a 250 m horizontal wind speed of \sim 5–

TORNOW ET AL. 3 of 12

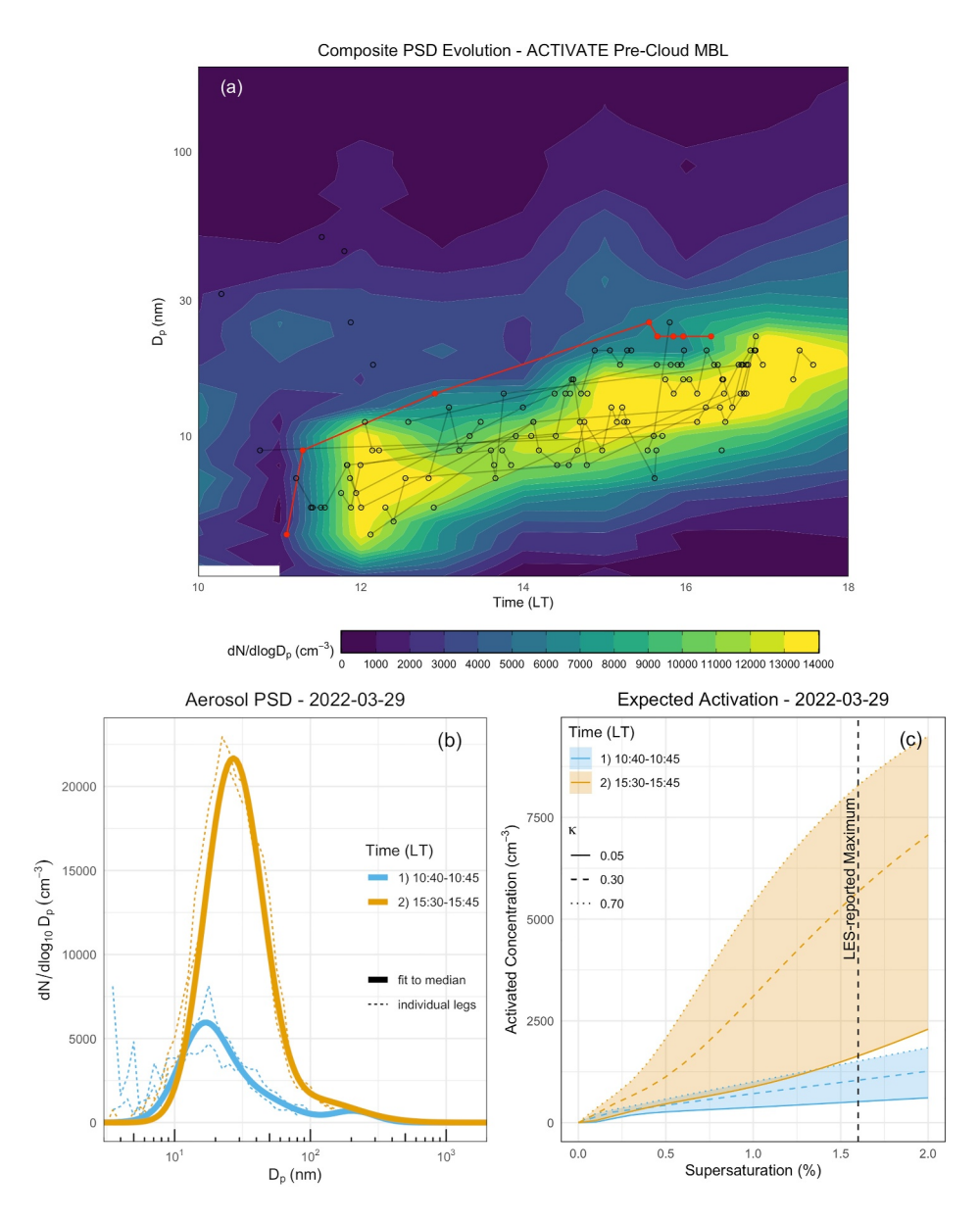


Figure 1. Aerosol properties in the pre-cloud marine boundary layer of postfrontal flights: (a) Composite of time-resolved particle size distribution of sizes between 3 and 150 nm for legs with a hot-to-cold ratios (i.e., the fraction of non-volatile CN_{10nm} over total CN_{10nm} , see Supporting Information S1 for more details) smaller than 0.25, overlaid with D_{p-max} (points and lines). (b) Exemplary PSDs at different times (colors) on 2022-03-29, also shown in red in panels (a). (c) Expected concentration of activated particles for three hygroscopicities (line types) applied to all aerosol (shadings show range between extremes).

25 m s⁻¹. MBL clouds formed over ocean with some distance from the coastline. Upwind of clouds (hereafter termed "pre-cloud") and inside the MBL spanning the polluted continental BL, this study seeks those particles comprising CCN under supersaturated conditions once advected farther downwind. Any change to the pre-cloud particle size distribution (PSD) is therefore expected to impact downwind cloud properties with some delay.

To understand the characteristics of the pre-cloud MBL, we examined in situ aerosol observations during flight legs that were classified as "MBL" (Text S1a in Supporting Information S1) and were mostly upwind of clouds, dL < 10 km (Text S1b in Supporting Information S1). PSDs collected from LAS and SMPS (Text S1c in Supporting Information S1) show a diurnal pattern indicative of NPF and growth, especially when filtered for a low fraction of non-volatile particles (Text S1c in Supporting Information S1). Figure 1a presents a PSD composite resolved by time-of-day and size for flight legs with a non-volatile fraction smaller than 25%. Up until 11

TORNOW ET AL. 4 of 12

LT (16 UTC), only small or moderate particle concentrations were seen, reaching maximum values of \sim 5,000 cm⁻³. Between 11 and 12 LT, particles of 3–10 nm reach an elevated concentration of >10,000 cm⁻³. Between 12 and 16 LT, the size range of elevated concentration shifts towards 10–30 nm, maintaining and sometimes increasing in particle concentration (values beyond 13,000 cm⁻³ are capped in Figure 1a).

About two thirds of the flights (47 out of 72 flights) show a small fraction of non-volatile particles (<0.25). Elevated nucleation mode particle concentrations and their growth are absent for non-volatile fractions greater than 0.25 (Figure S1 in Supporting Information S1). To highlight the size growth of newly formed particles, we overlay all flights' peak particle diameters with concentration exceeding $10,000 \, \mathrm{cm}^{-3}$ in Figure 1a (circles, 40 out of 72 flights) and connect multiple legs from the same date by lines. With few exceptions, line slopes are positive, indicating a persistent increase in nucleation and Aitken modal mean diameter. Measurements on 29 March 2022 (highlighted in red) showed the strongest increase in size, reaching $\sim 30 \, \mathrm{nm}$ at $\sim 16 \, \mathrm{LT}$ with concentrations greater than $20,000 \, \mathrm{cm}^{-3}$. We will examine this case more closely to understand implications for cloud properties.

While nucleation and Aitken mode concentrations stand out from the composite, there are also concentration increases in the accumulation mode size range (here defined as $D_p > 80$ nm), evidenced by progressively lighter shades in the upper third of Figure 1a. Most flights (63%, Tables S1 and S2 in Supporting Information S1) show an accumulation mode increase, here quantified through the change rate of CCN measured at a steady supersaturation (either 0.37 or 0.43%) that approximately translates into particle diameters \sim 70–90 nm. Accumulation mode number concentration changes appear unconnected to Aitken mode properties (see Table S3 in Supporting Information S1), lacking consistent correlations between changes and particle concentrations for $D_p > 10$ nm, CN_{10nm}, and diameters at peak density.

3.2. Implications for CCN

A priori it is unclear whether supersaturations inside postfrontal clouds are large enough to activate Aitken mode aerosol. By using 29 March 2022, the day showing an increase to the largest Aitken mode size, we infer maximum effects for the downwind cloud deck for any given supersaturation. Figure 1b compares PSDs from 10:40–10:45 LT (blue), a time with no indication of NPF (cf. Figure 1a) and comparatively lower concentrations (here up to $5,000~\rm cm^{-3}$) peaking at relatively small sizes (here $D_p \sim 15~\rm nm$), and $15:30–15:45~\rm LT$ (orange), a time of growth to $\sim 30~\rm nm$ and increased particle concentration, here exceeding $20,000~\rm cm^{-3}$. Like the multi-day composite, we also note increased concentrations in the size range around $D_p \sim 100~\rm nm$ from morning to afternoon.

In Figure 1b, the aerosol size distributions measured during individual legs from each timeframe (dotted lines) are well matched by their respective multi-modal fits to median values (thick solid lines, values provided in Table S4 in Supporting Information S1). We utilize these fits and simplified Koehler theory (Text S1d in Supporting Information S1) to calculate the expected number concentrations of activated aerosol per given supersaturation and hygroscopicity. Since hygroscopicity is unknown and CCN measurements, which would be essential to perform hygroscopicity-inferring CCN closure, were not available on the day of interest, we impose hygroscopicity. To capture extremes (e.g., Phillips et al., 2018), we perform calculations for $\kappa = 0.05$ and $\kappa = 0.70$. To capture activation for moderate hygroscopicity that appears typically under continental conditions (Figure 8 in Phillips et al., 2018), we also perform calculations for $\kappa = 0.30$. The resulting concentrations of activated particles are shown in Figure 1c.

At the 0.3% supersaturation of typical CCN measurements under wintertime conditions (Kirschler et al., 2022), activation of morning aerosol (blue) produces ~200 and 400 cm⁻³ for $\kappa = 0.05$ and $\kappa = 0.70$, respectively. The moderate hygroscopicity, $\kappa = 0.30$, falls in between with values of 300 cm⁻³. Afternoon activated aerosol increases to ~300 and 1,000 cm⁻³, respectively, again with $\kappa = 0.30$ falling in between the two with values of 650 cm⁻³. The difference at such moderate supersaturation stems solely from accumulation mode aerosol (not shown). At greater supersaturation, smaller aerosol modes also become activated. For example, at 1.6% supersaturation—a typical domain maximum value in preliminary LES (vertical dashed line)—morning aerosol produces ~500 and 1,500 cm⁻³ for $\kappa = 0.05$ and $\kappa = 0.70$, respectively, while afternoon aerosol results in ~1,600 and 8,300 cm⁻³, respectively. Accumulation-mode differences (i.e., 250 vs. 1,100 cm⁻³) that created CCN differences at lower supersaturation persist at greater supersaturations but the increased disparity at 1.6% compared to 0.3% now stems from activated Aitken mode aerosol (not shown). For $\kappa = 0.30$, concentrations at

TORNOW ET AL. 5 of 12

high supersaturations notably increase from $\sim 1,000$ and 5,700 cm⁻³, for morning and afternoon, respectively, as a result of the activation of smaller modes.

3.3. Implications for Cloud Properties

As demonstrated in Section 3.2, the changing aerosol PSD between morning and afternoon and the resulting impact on CCN concentrations depends on the prevalent hygroscopicity. That hygroscopicity should also impact the evolution of micro- and macro cloud properties farther downwind. Because a microphysical CCN closure was not possible for this day, we here perform a cloud macrophysical closure using Lagrangian LES and observational constraints.

Both of ACTIVATE's two flights on 29 March 2022 reached past the overcast into the broken cloud deck. As described in more detail in Text S1e in Supporting Information S1, we identify a trajectory that connects one of the farthest points at the latest time of the day with upwind pre-cloud conditions that roughly match the time of morning aerosol so as to initialize LES. Along this trajectory, we identify several flight legs that fall within a temporal (<60 min) and geospatial window (<100 km) and utilize any in situ or remote sensing measurements as observational constraints (Figure S4 in Supporting Information S1). In addition, we collocate instantaneous satellite observational constraints to the trajectory (Section 2.2), as done in previous work (Tornow et al., 2023). We note that RSP LWP retrievals (shown as "ACTIVATE (remote sensing)" in Figure 2) only capture cloud liquid paths, missing non-zero rain water paths. Meanwhile, MAC-LWP and LES mark cloud plus rain water. The three can only be compared where rain is absent, here guided by LES (marking rain-affected data points in gray in Figure 2).

Figure 2 shows three Lagrangian LES, one for each of low ($\kappa = 0.05$), moderate ($\kappa = 0.30$), and high hygroscopicity ($\kappa = 0.70$). Overlaid as symbols are available field campaign and satellite observational constraints. The three simulations show a similar evolution. Scene albedo (Figure 2a) increases as the cloud deck fills in (Figure 2b) and the LWP increases (Figure 2c). A decrease in albedo and maximum LWP roughly coincide with the onset of substantial rain (Figure 2d, RWP > 25 g m⁻²) and a cloud breakup, that is a decrease of cloud cover, thereafter. Ice water path (Figure 2e) and also frozen hydrometeor concentrations (Figure 2h) increase past the cloud breakup where the Hallett-Mossop secondary ice process is active in the model (not explicitly shown). This evolution is consistent with previous studies of similar conditions (Seethala et al., 2024; Tornow et al., 2021, 2023). Oscillations in most metrics stem from mesoscale cloud features approaching the domain size and prevail in a simulation with quadrupled size (Figures S8 and S9 in Supporting Information S1).

The main difference between the simulations is cloud droplet number concentration (Figure 2g), reaching peak concentrations of 250, 400, and 500 cm^{-3} for low, moderate, and high hygroscopicity, respectively. The roughly doubled concentrations from low to high hygroscopicity modify the evolution by prolonging the LWP buildup (peak values reached at \sim 9 hr compared to \sim 7.5 hr under low hygroscopicity), delaying rain onset and subsequent cloud breakup (cloud cover dropping below 75% at 12.5 hr compared to 9 hr under low hygroscopicity). In effect, scene albedo differs around 9 hr by up to \sim 0.4 (i.e., a 50% reduction when moving from high to low hygroscopicity).

Next, we compare simulations with observations. GOES-16 cloud cover (Figure 2b) shows earlier (later) cloud formation than high (low) hygroscopicity simulations, aligning best with moderate hygroscopicity which captures a cloud breakup after \sim 10 hr. MAC-LWP (Figure 2c) initially exceeds simulations but aligns at 3 and 7 hr, then dips after \sim 9 hr—again matching low and moderate hygroscopicity simulations, which drop to observed levels after \sim 10 and 11 hr, respectively. After 13 hr, all simulations converge and agree with most MAC-LWP values, indicating realistic condensate phase partitioning though IWP lacks constraints. RSP retrievals (Cairns et al., 1999) match simulated values at 3–7 hr then align with MAC-LWP at 8–10 hr despite likely precipitation effects (Figure 2d). Droplet number concentrations from in situ probes and from RSP (Figure 2g) span a wide range but cluster around values from low and moderate hygroscopicity simulations. in situ frozen hydrometeor concentrations (Figure 2h) roughly match simulated N_i levels around 4–6 hr and also increase between 7 and 10 hr, aligning well with simulations. Due to variability in in situ field campaign data we rely on RSP and satellite data. These suggest that low or moderate hygroscopicity best reproduces observed cloud properties. A case with weaker aerosol growth but available CCN measurements also supports moderate hygroscopicity (Figure S5 in Supporting Information S1). Section 4 will discuss the plausibility of either hygroscopicity and compare against recent literature.

TORNOW ET AL. 6 of 12

.com/doi/10.1029/2025GL116020 by Disch Zentrum F. Luft-U. Raum Fahrt In D. Helmholtz Gemein., Wiley Online Library on [25/09/2025]. See the Terms

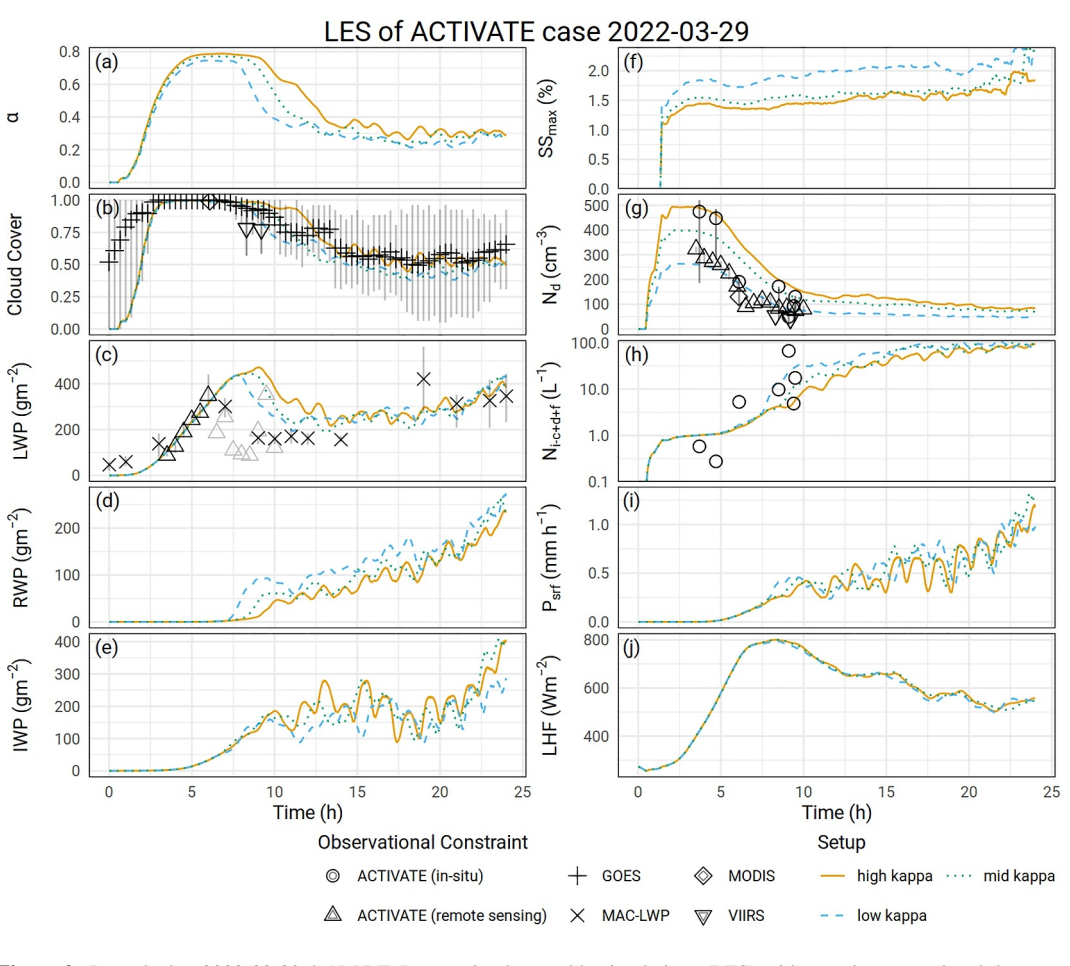


Figure 2. Launched at 2022-03-29 4 AM LT, Lagrangian large eddy simulations (LES) with morning aerosol and three hygroscopicities (line types and colors) and observed properties (symbols) from ACTIVATE flights and satellite platforms, showing the following properties: (a) pseudo-albedo, (b) cloud cover, (c) liquid water path including cloud and rain, (d) rain water path, (e) ice water path, (f) domain-maximum supersaturation, (g) condensate-weighted domain-average cloud droplet number concentration, (h) ice number concentration, (i) surface precipitation rate, and (j) surface turbulent latent heat flux, some with observational constraints from satellite and ACTIVATE flights (black symbols). LWP values in gray mark RSP-based CWP retrievals under suspected precipitation, as suggested by LES (see text). Vertical lines mark the interquartile range of observed quantities, except for cloud cover where bars span 2.5th to 97.5th percentiles.

To isolate the impact of evolving aerosol PSD onto clouds, we performed simulations assuming other conditions constant, though meteorology was not steady (not shown). Without observational constraints, we use a moderate hygroscopicity ($\kappa = 0.30$) to compare morning (blue) and afternoon (orange) aerosol configurations. Results show that afternoon aerosol increase droplet number concentration (Figure 3g), prolong LWP buildup, delay rain onset (Figure 3d), and reduce cloud cover later (\sim 16 hr vs. \sim 11 hr). Scene albedo differences peak between 10 and 17 LT, reaching up to 0.35—an increase of \sim 90% when switching from morning to afternoon aerosol.

To understand which aerosol modes drive the above effect, we analyze a hybrid simulation combining afternoon accumulation mode aerosol with morning aerosol nucleation and Aitken modes (green, Table S4 in Supporting Information S1). This setup closely matches the afternoon-only simulation, except for an earlier cloud breakup and albedo reduction (Figure 3a), indicating that accumulation mode aerosol dominates cloud and precipitation responses. Peak droplet number concentrations (\sim 700 cm $^{-3}$) in both simulations reflect only partial activation of available aerosol accumulation mode aerosol. In contrast, the morning aerosol (blue) reaches 400 cm $^{-3}$ suggesting Aitken mode activation due to higher supersaturation. Afternoon accumulation mode aerosol reduces domain-maximum supersaturations (Figure 2f), suppressing Aitken mode activation—a behavior specific to low and moderate hygroscopicity. Under high hygroscopicity ($\kappa = 0.70$), droplet number concentration increase up to 1,000 cm $^{-3}$ in the afternoon, though macroscopic cloud changes remain modest. Simulations with low

TORNOW ET AL. 7 of 12

.com/doi/10.1029/2025GL116020 by Disch Zentrum F. Luft-U. Raum Fahrt In D. Helmholtz Gemein., Wiley Online Library on [25/09/2025]. See the Term

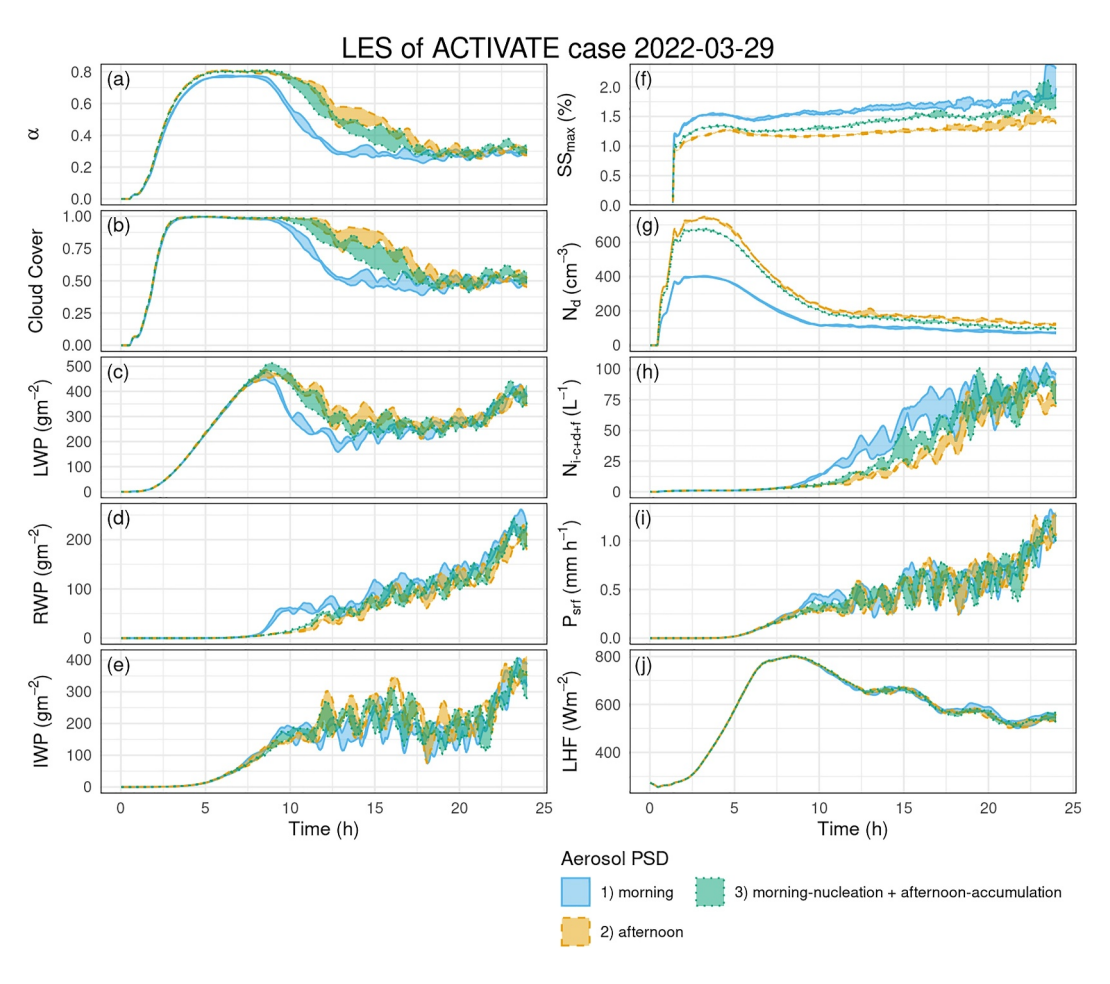


Figure 3. Similar to Figure 2 where large eddy simulations runs with different aerosol size distributions and moderate hygroscopicity are performed: using (1) a morning configuration (already shown in Figure 2 as blue dashed line), (2) an afternoon configuration, and (3) a blend using the nucleation and Aitken mode properties of (1) and the accumulation mode properties of (2). The configuration is specified in Table S3 in Supporting Information S1.

hygroscopicity ($\kappa = 0.05$) show similar results but with lower N_d . A case study from 2022-02-19 shows negligible cloud differences (Figure S6 in Supporting Information S1) due to weaker aerosol changes (Figure S5 in Supporting Information S1).

In essence, we performed a cloud macroscopic closure to infer low or moderate hygroscopicity in morning aerosol conditions to be more plausible. For a changing aerosol PSD from morning to afternoon, the response in cloud properties is governed by the increase in accumulation mode concentrations, rendering NPF-induced changes in nucleation and Aitken mode aerosol largely inconsequential. Results are not sensitive to hygroscopicity insofar as the diurnal evolution of the accumulation mode number concentration remains a significantly greater factor than the nucleation and Aitken mode evolution over a wide range of assumed κ values.

4. Discussion

The ACTIVATE domain we focused on is expected to be more polluted than other extratropical regions and high latitudes. For example, the NAAMES (North Atlantic Aerosols and Marine Ecosystems Study, Behrenfeld et al., 2019) deployments a few hundred kilometers farther north show a similar multi-modal aerosol but of an order of magnitude smaller aerosol number concentrations with substantial contributions from sea spray and sulfate particles at a similar time of year (Sanchez et al., 2018). The large number concentration gap could stem from anthropogenic emissions, for example, from coastal cities and these emissions are expected to be elevated during post-frontal passages, in particular cold-air outbreaks. Since accumulation mode concentrations are orders of magnitude smaller at higher latitudes, clouds can activate Aitken mode aerosol (Bulatovic et al., 2021).

TORNOW ET AL. 8 of 12

It remains unclear whether accumulation mode changes are connected to NPF. Studies using Earth system models (e.g., Zhao et al., 2024) present little to no such changes. Novel LES has demonstrated an efficient transport from smaller to larger modes by activation and in-cloud processing (I. L. McCoy et al., 2024). Such transport can be excluded here as we examine PSD evolution in the pre-cloud area (i.e., cloud-free conditions upwind of the cloud deck).

Is either a low or moderate aerosol hygroscopicity plausible? We note multiple pieces of evidence in favor: (a) a large organic mass fraction (detected for particles $D_p \sim 150$ –300 nm) likely stemming from aforementioned anthropogenic emissions, (b) a short exposure to high-hygroscopicity sources, such as sea-spray emissions, that should mostly contain sea-salt during off-summer months (e.g., Sanchez et al., 2018) and dominate MBL aerosol farther downwind, and (c) the cloud macro-physical response shown here, that would have appeared differently and therefore deviated from observational benchmark for greater hygroscopicity (cf. Figure 2). Previous studies have also found a low to moderate aerosol hygroscopicity in a range of environments, including springtime rural areas ($\kappa = 0.05$ –0.30 for $D_p < 50$ nm, Fridlind et al., 2017; Mahish & Collins, 2017), continental air arriving at a northeast Pacific site ($\kappa = 0.1$ –0.2, Schulze et al., 2020), a forested site ($\kappa = 0.1$ –0.2 for particles $D_p = 50$ nm, Levin et al., 2014), urban sites in South Korea ($\kappa = 0.05$ –0.25 for $D_p < 50$ nm, Kim et al., 2020) and Beijing ($\kappa = 0.1$ –0.2 for $D_p < 50$ nm, Fan et al., 2020), and a polluted site in northern China ($\kappa = 0.05$ –0.15, Kuang et al., 2020), which all stand in stark contrast to the marine environment that typically shows greater values ($\kappa \ge 0.4$, e.g., Kuang et al., 2020).

Our simulations demonstrate the importance of considering multiple modes of aerosol in simulations. Unless accumulation mode aerosol concentrations fully create an updraft-limited regime by themselves (i.e., afternoon conditions of the case studied here), supersaturations are typically great enough to activate smaller modes. Such activation acts just like activating a larger concentration of accumulation mode aerosol: the increased N_d acts to delay the onset of rain and decrease rain rates, which results in an elevated albedo. A more sophisticated treatment of multi-modal aerosol (I. L. McCoy et al., 2024) mimics cloud processing and the concomitant transfer from smaller to larger aerosol modes, which is expected to increase the role of transferred aerosol where supersaturations may decrease.

5. Conclusions

This paper examines the postfrontal MBL over the Northwest Atlantic, probed over the course of several years via ACTIVATE flight campaign deployments and supports the following conclusions:

- 1. With a focus on MBL portions upwind of cloud formation, we reveal a persistent morning to afternoon pattern with size growth of nucleation mode into Aitken mode aerosol, likely triggered by NPF arising from anthropogenic emissions. In addition, we often find a concomitant increase in accumulation mode concentrations (Figure 1a).
- 2. Based on the day of strongest nucleation-to-Aitken mode size growth, we perform quasi-Lagrangian LES to assess the impact to the downwind cloud field. Constrained by ACTIVATE flight measurements and retrievals from geostationary and low-earth orbiting satellites, we establish that multi-modal aerosol representing pre-NPF conditions are of low or moderate aerosol hygroscopicity (Figure 2).
- 3. An idealized configuration switching to a post-NPF aerosol size distribution shows a delayed precipitation onset and a prolonged phase of increased albedo, primarily caused by the increased accumulation mode concentration that inhibits activation of smaller particles, despite their increased diameter, thereby fashioning an updraft-limited regime (Figure 3).
- 4. Postfrontal clouds in less polluted regions should be more susceptible to NPF-shaped changes to the smaller aerosol modes (Section 4).
- 5. Considering multiple lognormal aerosol modes is pivotal to capture aerosol-cloud-precipitation interaction in postfrontal clouds (Section 4).

Data Availability Statement

ACTIVATE flight measurements comprise in situ measurements of clouds (NASA/LaRC/SD/ASDC, 2023, public access, no restrictions via https://asdc.larc.nasa.gov/soot/search, select "ACTIVATE" for campaign and "HU25" for platform and find "N-ice_2DS" and "N_FCDP" for ice and liquid number concentrations,

TORNOW ET AL. 9 of 12

respectively) and aerosol (NASA/LARC/SD/ASDC, 2021, find "Array: SMPS_Bin01-SMPS_Bin30" and "Array: LAS_Bin01-LAS_Bin26" aerosol number size distributions as well as "CCN_SS" for CCN concentrations), and remote sensing products (NASA/LaRC/SD/ASDC, 2021b, select "ACTIVATE" for campaign and "KingAir" for platform and look for "COT" and "Reff" cloud optical thickness and cloud droplet effective radius, respectively). GOES SatCorps retrievals (NASA/LaRC/SD/ASDC, 2021a) are available via the data archive at ACTIVATE's field data repository https://asdc.larc.nasa.gov/project/ACTIVATE (NASA/LaRC/SD/ASDC, 2019b), and also publicly via https://asdc.larc.nasa.gov/soot/search (NASA/LaRC/SD/ASDC, 2019a). Other satellite data (Platnick et al., 2015, 2017) are available via https://search.earthdata.nasa.gov/ (NASA/GSFC/ESPD, 2024). Hourly MAC-LWP retrievals (Elsaesser et al., 2017) are available upon request. LES domain-averages are uploaded https://doi.org/10.5281/zenodo.15001340 (Tornow, Ackerman, & Fridlind, 2025).

Acknowledgments

This work was supported by ACTIVATE, a NASA Earth Venture Suborbital-3 (EVS-3) investigation funded by NASA's Earth Science Division and managed through the Earth System Science Pathfinder Program Office Division (Grant 80NSSC19K044). The authors thank the ACTIVATE team for helpful discussion and for support with measurements and quality control. AMF and GSE were supported by the NASA Modeling, Analysis and Prediction Program, which supports development of the NASA ModelE climate model. PZ gratefully acknowledges support from NASA Grant 80NSSC19K0390. CV and SK were supported by DFG SPP-1294 HALO under project 522359172 and by the European Union's Horizon Europe program through the Single European Sky ATM Research 3 Joint Undertaking projects CONCERTO (Grant 101114785) and CICONIA (Grant 101114613). We thank two anonymous reviewers for their constructive feedback that helped to improve this paper.

References

- Behrenfeld, M. J., Moore, R. H., Hostetler, C. A., Graff, J., Gaube, P., Russell, L. M., et al. (2019). The North Atlantic aerosol and marine ecosystem study (NAAMES): Science motive and mission overview. Frontiers in Marine Science, 6, 122. https://doi.org/10.3389/fmars.2019.
- Bulatovic, I., Igel, A. L., Leck, C., Heintzenberg, J., Riipinen, I., & Ekman, A. M. (2021). The importance of Aitken mode aerosol particles for cloud sustenance in the summertime high Arctic—a simulation study supported by observational data. *Atmospheric Chemistry and Physics*, 21(5), 3871–3897. https://doi.org/10.5194/acp-21-3871-2021
- Burton, S. P., Hostetler, C. A., Cook, A. L., Hair, J. W., Seaman, S. T., Scola, S., et al. (2018). Calibration of a high spectral resolution lidar using a Michelson interferometer, with data examples from ORACLES. *Applied Optics*, 57(21), 6061–6075. https://doi.org/10.1364/AO.57.006061
- Cairns, B., Russell, E. E., & Travis, L. D. (1999). Research scanning polarimeter: Calibration and ground-based measurements. In D. H. Goldstein & D. B. Chenault (Eds.), *Polarization: Measurement, analysis, and remote sensing II* (Vol. 3754, pp. 186–196). SPIE. https://doi.org/10.1117/12.366329
- Comstock, K. K., Wood, R., Yuter, S. E., & Bretherton, C. S. (2004). Reflectivity and rain rate in and below drizzling stratocumulus. *Quarterly Journal of the Royal Meteorological Society: A journal of the atmospheric sciences, applied meteorology and physical oceanography, 130*(603), 2891–2918. https://doi.org/10.1256/qj.03.187
- Corral, A. F., Choi, Y., Crosbie, E., Dadashazar, H., DiGangi, J. P., Diskin, G. S., et al. (2022). Cold air outbreaks promote new particle formation off the U.S. East Coast. *Geophysical Research Letters*, 49(5), e2021GL096073. https://doi.org/10.1029/2021GL096073
- Eastman, R., McCoy, I. L., & Wood, R. (2022). Wind, rain, and the closed to open cell transition in subtropical marine stratocumulus. *Journal of Geophysical Research: Atmospheres*, 127(20), e2022JD036795. https://doi.org/10.1029/2022JD036795
- Elsaesser, G. S., O'Dell, C. W., Lebsock, M. D., Bennartz, R., Greenwald, T. J., & Wentz, F. J. (2017). The multisensor advanced climatology of liquid water path (MAC-LWP). *Journal of Climate*, 30(24), 10193–10210. https://doi.org/10.1175/JCLI-D-16-0902.1
- Fan, X., Liu, J., Zhang, F., Chen, L., Collins, D., Xu, W., et al. (2020). Contrasting size-resolved hygroscopicity of fine particles derived by HTDMA and HR-ToF-AMS measurements between summer and winter in Beijing: The impacts of aerosol aging and local emissions. Atmospheric Chemistry and Physics, 20(2), 915–929. https://doi.org/10.5194/acp-20-915-2020
- Fridlind, A. M., Li, X., Wu, D., van Lier-Walqui, M., Ackerman, A. S., Tao, W.-K., et al. (2017). Derivation of aerosol profiles for MC3E convection studies and use in simulations of the 20 May squall line case. *Atmospheric Chemistry and Physics*, 17(9), 5947–5972. https://doi.org/10.5194/acp-17-5947-2017
- Gordon, H., Kirkby, J., Baltensperger, U., Bianchi, F., Breitenlechner, M., Curtius, J., et al. (2017). Causes and importance of new particle formation in the present-day and preindustrial atmospheres. *Journal of Geophysical Research: Atmospheres*, 122(16), 8739–8760. https://doi.org/10.1002/2017JD026844
- Grossman, R. L., & Betts, A. K. (1990). Air–sea interaction during an extreme cold air outbreak from the eastern coast of the United States. Monthly Weather Review, 118(2), 324–342. https://doi.org/10.1175/1520-0493(1990)118(0324:AIDAEC)2.0.CO;2
- Hersbach, H., Bell, B., Berrisford, P., Hirahara, S., Horányi, A., Muñoz-Sabater, J., et al. (2020). The ERA5 global reanalysis. *Quarterly journal of the royal meteorological society*, 146(730), 1999–2049. https://doi.org/10.1002/qji.3803
- Kim, N., Yum, S. S., Park, M., Park, J. S., Shin, H. J., & Ahn, J. Y. (2020). Hygroscopicity of urban aerosols and its link to size-resolved chemical composition during spring and summer in Seoul, Korea. Atmospheric Chemistry and Physics, 20(19), 11245–11262. https://doi.org/10.5194/acp-20-11245-2020
- Kirschler, S., Voigt, C., Anderson, B., Campos Braga, R., Chen, G., Corral, A. F., et al. (2022). Seasonal updraft speeds change cloud droplet number concentrations in low-level clouds over the western North Atlantic. *Atmospheric Chemistry and Physics*, 22(12), 8299–8319. https://doi.org/10.5194/acp-22-8299-2022
- Korolev, A., Qu, Z., Milbrandt, J., Heckman, I., Cholette, M., Wolde, M., et al. (2024). High ice water content in tropical mesoscale convective systems (A conceptual model). Atmospheric Chemistry and Physics, 24(20), 11849–11881. https://doi.org/10.5194/acp-24-11849-2024
- Kuang, Y., He, Y., Xu, W., Zhao, P., Cheng, Y., Zhao, G., et al. (2020). Distinct diurnal variation in organic aerosol hygroscopicity and its relationship with oxygenated organic aerosol. Atmospheric Chemistry and Physics, 20(2), 865–880. https://doi.org/10.5194/acp-20-865-2020
- relationship with oxygenated organic aerosol. *Atmospheric Chemistry and Physics*, 20(2), 863–880. https://doi.org/10.5194/acp-20-865-2020 Levin, E., Prenni, A., Palm, B., Day, D., Campuzano-Jost, P., Winkler, P., et al. (2014). Size-resolved aerosol composition and its link to hygroscopicity at a forested site in Colorado. *Atmospheric Chemistry and Physics*, 14(5), 2657–2667. https://doi.org/10.5194/acp-14-2657-2014
- Liu, H., Zhang, B., Moore, R. H., Ziemba, L. D., Ferrare, R. A., Choi, H., et al. (2024). Tropospheric aerosols over the western North Atlantic Ocean during the winter and summer campaigns of ACTIVATE 2020: Life cycle, transport, and distribution. EGUsphere, 2024, 1–68. https://doi.org/10.5194/egusphere-2024-1127
- Mahish, M., & Collins, D. (2017). Analysis of a multi-year record of size-resolved hygroscopicity measurements from a rural site in the US. Aerosol and Air Quality Research, 17(6), 1489–1500. https://doi.org/10.4209/aaqr.2016.10.0443
- McCoy, D. T., Frazer, M. E., Mülmenstädt, J., Tan, I., Terai, C. R., & Zelinka, M. D. (2023). Extratropical cloud feedbacks. In Clouds and their climatic impacts (pp. 133–157). American Geophysical Union (AGU). https://doi.org/10.1002/9781119700357.ch6
- McCoy, I. L., Wyant, M. C., Blossey, P. N., Bretherton, C. S., & Wood, R. (2024). Aitken mode aerosols buffer decoupled mid-latitude boundary layer clouds against precipitation depletion. *Journal of Geophysical Research: Atmospheres*, 129(12), e2023JD039572. https://doi.org/10.1029/2023JD039572

TORNOW ET AL. 10 of 12

- Minnis, P., & Heck, P. (2012). GOES-R advanced baseline imager (ABI) algorithm theoretical basis document for nighttime cloud optical depth, cloud particle size, cloud ice water path, and cloud liquid water path. NOAA NESDIS, Center for Satellite Applications and Research. Retrieved from https://www.star.nesdis.noaa.gov/goesr/documents/ATBDs/Baseline/ATBD_GOES-R_Cloud_NCOMP_v3.0_Jul2012.pdf
- Namdari, S., Ajayi, T., Choi, Y., Crosbie, E. C., DiGangi, J. P., Diskin, G. S., et al. (2024). A comprehensive analysis of new particle formation across the northwest Atlantic: Analysis of ACTIVATE airborne data. Atmospheric Environment, 338, 120831. https://doi.org/10.1016/j.atmosenv.2024.120831
- NASA/GSFC/ESPD. (2024). Earthdata search. Retrieved from https://www.earthdata.nasa.gov
- NASA/LaRC/SD/ASDC. (2019a). Aerosol cloud meTeorology interactions oVer the western ATlantic experiment. NASA Langley Atmospheric Science Data Center DAAC. Retrieved from https://asdc.larc.nasa.gov/soot/search
- NASA/LaRC/SD/ASDC. (2019b). Sub-orbital order tool (SOOT). NASA Langley Atmospheric Science Data Center DAAC. https://doi.org/10.5067/SUBORBITAL/ACTIVATE/DATA001
- NASA/LARC/SD/ASDC. (2021). ACTIVATE Falcon in situ aerosol data [Dataset]. NASA Langley Atmospheric Science Data Center DAAC. https://doi.org/10.5067/ASDC/ACTIVATE_Aerosol_AircraftInSitu_Falcon_Data_1
- NASA/LaRC/SD/ASDC. (2021a). ACTIVATE GOES-16 supplementary data products [Dataset]. NASA Langley Atmospheric Science Data Center DAAC. https://doi.org/10.5067/ASDC/SUBORBITAL/ACTIVATE-Satellite_1
- NASA/LaRC/SD/ASDC. (2021b). ACTIVATE king air aerosol and cloud remotely sensed data [Dataset]. NASA Langley Atmospheric Science Data Center DAAC. https://doi.org/10.5067/ASDC/ACTIVATE_AerosolCloud_AircraftRemoteSensing_KingAir_Data_1
- NASA/LaRC/SD/ASDC. (2023). ACTIVATE Falcon in situ cloud data [Dataset]. NASA Langley Atmospheric Science Data Center DAAC. https://doi.org/10.5067/ASDC/ACTIVATE Cloud AircraftInSitu Falcon Data 1
- Painemal, D., & Zuidema, P. (2011). Assessment of MODIS cloud effective radius and optical thickness retrievals over the Southeast Pacific with VOCALS-REx in situ measurements. *Journal of Geophysical Research*, 116(D24), https://doi.org/10.1029/2011JD016155
- Park, J. M., McComiskey, A. C., Painemal, D., & Smith Jr, W. L. (2024). Long-term trends in aerosols, low clouds, and large-scale meteorology over the western north Atlantic from 2003 to 2020. *Journal of Geophysical Research: Atmospheres*, 129(11), e2023JD039592. https://doi.org/ 10.1029/2023JD039592
- Phillips, B. N., Royalty, T., Dawson, K., Reed, R., Petters, M., & Meskhidze, N. (2018). Hygroscopicity-and size-resolved measurements of submicron aerosol on the East Coast of the United States. *Journal of Geophysical Research: Atmospheres*, 123(3), 1826–1839. https://doi.org/ 10.1002/2017JD027702
- Platnick, S., Ackerman, S. A., King, M. D., Meyer, K., Menze, W. P., Holz, R. E., et al. (2015). MODIS atmosphere L2 cloud product (06_L2) [Dataset]. NASA MODIS Adaptive Processing System, Goddard Space Flight Center. https://doi.org/10.5067/MODIS/MOD06_L2.006
- Platnick, S., Ackerman, S. A., King, M. D., Meyer, K., Menze, W. P., Holz, R. E., et al. (2017). VIIRS atmosphere L2 cloud properties product. Version-1 [Dataset]. NASA Level-1 and Atmosphere Archive & Distribution System (LAADS) Distributed Active Archive Center (DAAC), Goddard Space Flight Center. https://doi.org/10.5067/VIIRS/CLDPROP_L2_VIIRS_SNPP.011
- Sanchez, K. J., Chen, C.-L., Russell, L. M., Betha, R., Liu, J., Price, D. J., et al. (2018). Substantial seasonal contribution of observed biogenic sulfate particles to cloud condensation nuclei. *Scientific Reports*, 8(1), 3235. https://doi.org/10.1038/s41598-018-21590-9
- Sanchez, K. J., Painemal, D., Brown, M. D., Crosbie, E. C., Gallo, F., Hair, J. W., et al. (2023). Multi-campaign ship and aircraft observations of marine cloud condensation nuclei and droplet concentrations. Scientific Data, 10(1), 471. https://doi.org/10.1038/s41597-023-02372-z
- Schulze, B., Charan, S., Kenseth, C., Kong, W., Bates, K., Williams, W., et al. (2020). Characterization of aerosol hygroscopicity over the Northeast Pacific Ocean: Impacts on prediction of CCN and stratocumulus cloud droplet number concentrations. *Earth and Space Science*, 7(7), e2020EA001098. https://doi.org/10.1029/2020EA001098
- Seethala, C., Zuidema, P., Kirschler, S., Voigt, C., Cairns, B., Crosbie, E. C., et al. (2024). Microphysical evolution in mixed-phase midlatitude marine cold-air outbreaks. *Journal of the Atmospheric Sciences*, 81(10), 1725–1747. https://doi.org/10.1175/JAS-D-23-0203.1
- Seidel, J. S., Kiselev, A. A., Keinert, A., Stratmann, F., Leisner, T., & Hartmann, S. (2024). Secondary ice production No evidence of efficient rime-splintering mechanism. Atmospheric Chemistry and Physics, 24(9), 5247–5263. https://doi.org/10.5194/acp-24-5247-2024
- Sorooshian, A., Alexandrov, M. D., Bell, A. D., Bennett, R., Betito, G., Burton, S. P., et al. (2023). Spatially coordinated airborne data and complementary products for aerosol, gas, cloud, and meteorological studies: The NASA ACTIVATE dataset. *Earth System Science Data*, 15(8), 3419–3472. https://doi.org/10.5194/essd-15-3419-2023
- Sorooshian, A., Anderson, B., Bauer, S. E., Braun, R. A., Cairns, B., Crosbie, E., et al. (2019). Aerosol-cloud-meteorology interaction airborne field investigations: Using lessons learned from the US West Coast in the design of ACTIVATE off the US East Coast. *Bulletin of the American Meteorological Society*, 100(8), 1511–1528. https://doi.org/10.1175/BAMS-D-18-0100.1
- Sorooshian, A., Siu, L. W., Butler, K., Brunke, M. A., Cairns, B., Chellappan, S., et al. (2025). The NASA ACTIVATE Mission. Bulletin of the American Meteorological Society, BAMS-D-24-0136.1. https://doi.org/10.1175/BAMS-D-24-0136.1
- Tornow, F., Ackerman, A., & Fridlind, A. (2025a). DHARMA LES output of marine cold-air outbreak event on 2022-03-29 [Dataset]. Zenodo. https://doi.org/10.5281/zenodo.15001341
- Tornow, F., Ackerman, A. S., & Fridlind, A. M. (2021). Preconditioning of overcast-to-broken cloud transitions by riming in marine cold air outbreaks. *Atmospheric Chemistry and Physics*, 21(15), 12049–12067. https://doi.org/10.5194/acp-21-12049-2021
- Tornow, F., Ackerman, A. S., Fridlind, A. M., Cairns, B., Crosbie, E. C., Kirschler, S., et al. (2022). Dilution of boundary layer cloud condensation nucleus concentrations by free tropospheric entrainment during marine cold air outbreaks. *Geophysical Research Letters*, 49(11), e2022GL098444. https://doi.org/10.1029/2022GL098444
- Tornow, F., Ackerman, A. S., Fridlind, A. M., Tselioudis, G., Cairns, B., Painemal, D., & Elsaesser, G. (2023). On the impact of a dry intrusion driving cloud-regime transitions in a midlatitude cold-air outbreak. *Journal of the Atmospheric Sciences*, 80(12), 2881–2896. https://doi.org/10.1175/JAS-D-23-0040.1
- Tornow, F., Fridlind, A., Tselioudis, G., Cairns, B., Ackerman, A., Chellappan, S., et al. (2025b). Measurement report: A survey of meteorological and cloud properties during ACTIVATE's postfrontal flights and their suitability for Lagrangian case studies. *Atmospheric Chemistry and Physics*, 25(9), 5053–5074. https://doi.org/10.5194/acp-25-5053-2025
- Tselioudis, G., Rossow, W. B., Jakob, C., Remillard, J., Tropf, D., & Zhang, Y. (2021). Evaluation of clouds, radiation, and precipitation in CMIP6 models using global weather states derived from ISCCP-H cloud property data. *Journal of Climate*, 34(17), 7311–7324. https://doi.org/10.1175/JCLI-D-21-0076.1
- Wood, R. (2005). Drizzle in stratiform boundary layer clouds. Part II: Microphysical aspects. Journal of the Atmospheric Sciences, 62(9), 3034–3050. https://doi.org/10.1175/JAS3530.1
- Wood, R., Stemmler, J. D., Rémillard, J., & Jefferson, A. (2017). Low-CCN concentration air masses over the eastern North Atlantic: Seasonality, meteorology, and drivers. *Journal of Geophysical Research: Atmospheres*, 122(2), 1203–1223. https://doi.org/10.1002/2016JD025557

TORNOW ET AL. 11 of 12



Geophysical Research Letters

- 10.1029/2025GL116020
- Wyant, M. C., Bretherton, C. S., Rand, H. A., & Stevens, D. E. (1997). Numerical simulations and a conceptual model of the stratocumulus to trade cumulus transition. *Journal of the Atmospheric Sciences*, 54(1), 168–192. https://doi.org/10.1175/1520-0469(1997)054(0168: NSAACM)2.0.CO;2
- Yamaguchi, T., Feingold, G., & Kazil, J. (2017). Stratocumulus to cumulus transition by drizzle. *Journal of Advances in Modeling Earth Systems*, 9(6), 2333–2349. https://doi.org/10.1002/2017MS001104
- Zelinka, M. D., Myers, T. A., McCoy, D. T., Po-Chedley, S., Caldwell, P. M., Ceppi, P., et al. (2020). Causes of higher climate sensitivity in CMIP6 models. *Geophysical Research Letters*, 47(1), e2019GL085782. https://doi.org/10.1029/2019GL085782
- Zhao, B., Donahue, N. M., Zhang, K., Mao, L., Shrivastava, M., Ma, P.-L., et al. (2024). Global variability in atmospheric new particle formation mechanisms. *Nature*, 631(8019), 98–105. https://doi.org/10.1038/s41586-024-07547-1

References From the Supporting Information

- Abdul-Razzak, H., & Ghan, S. J. (2000). A parameterization of aerosol activation: 2. Multiple aerosol types. *Journal of Geophysical Research*, 105(D5), 6837–6844. https://doi.org/10.1029/1999JD901161
- Kirschler, S., Voigt, C., Anderson, B. E., Chen, G., Crosbie, E. C., Ferrare, R. A., et al. (2023). Overview and statistical analysis of boundary layer clouds and precipitation over the western North Atlantic Ocean. *Atmospheric Chemistry and Physics*, 23(18), 10731–10750. https://doi.org/10.5194/acp-23-10731-2023
- Knop, I., Bansmer, S. E., Hahn, V., & Voigt, C. (2021). Comparison of different droplet measurement techniques in the Braunschweig Icing Wind Tunnel. Atmospheric Measurement Techniques, 14(2), 1761–1781. https://doi.org/10.5194/amt-14-1761-2021
- Lawson, R. P., O'Connor, D., Zmarzly, P., Weaver, K., Baker, B., Mo, Q., & Jonsson, H. (2006). The 2D-S (stereo) probe: Design and preliminary tests of a new airborne, high-speed, high-resolution particle imaging probe. *Journal of Atmospheric and Oceanic Technology*, 23(11), 1462–1477. https://doi.org/10.1175/JTECH1927.1
- Morrison, H., & Grabowski, W. W. (2008). Modeling supersaturation and subgrid-scale mixing with two-moment bulk warm microphysics. *Journal of the Atmospheric Sciences*, 65(3), 792–812. https://doi.org/10.1175/2007JAS2374.1

TORNOW ET AL. 12 of 12